and PTP1B$^{D/A}$, even in cells stimulated for 30 min with EGF or PDGF (Fig. 2C).

The data above indicated that after growth factor stimulation, PTP1B interacts with internalized RTKs [Fig. 2; Web fig. 2 (*13*)]. To determine whether RTK-PTP1B interactions occur within the punctate structures we observed in the ER, we generated a high-resolution 3D image of the sites of RTK-PTP1B interaction in cells. We monitored localization of these molecules by confocal microscopy (Fig. 3A) and their interactions by FRET using the acceptor photobleaching approach (Fig. 3B), which measures the increased intensity of a donor fluorophore that follows photobleaching of the acceptor (*24*). After 30 min of growth factor stimulation, high FRET efficiencies were observed exclusively on the punctate structures [Fig. 3B; Web fig. 3 and movies 1 and 2 (*13*)], where PTP1B and the RTKs colocalize [Fig. 3A; Web fig. 3 and movies 1 and 2 (*13*)].

Thus, RTK interactions with the catalytic center of PTP1B—and, by inference, RTK dephosphorylation by PTP1B—require receptor endocytosis, occur at specific times after growth factor activation, and take place in discrete spatial locations within the cell. ER-anchored PTP1B specifically dephosphorylates endocytosed RTKs, thereby contributing to RTK signal termination. Other PTPs may function at the plasma membrane to prevent gratuitous RTK activation or activation by subthreshold levels of growth factor. Ligand-induced RTK activation overcomes these local PTPs, possibly by promoting the production of reactive oxygen species that can transiently oxidize the essential catalytic cysteinyl residue in PTPs (*25*). Receptor endocytosis also may play an important role in potentiating RTK activation, by promoting separation between RTKs and plasma membrane–proximal PTPs. Although PTPs play a critical role in RTK signal modulation, specific seryl phosphorylation events (*26*) and RTK targeting to lysosomes, a process that involves RTK ubiquitination (*27*, *28*), also are important RTK-inactivation mechanisms. From our FLIM data, we estimate that about 20% of all the EGFR-GFP molecules in a cell exhibit FRET with PTP1B (at 30 min after EGF stimulation). About 35% of total EGFR-GFP molecules are active under similar conditions (*18*). Taken together, these data imply that a high percentage of activated RTKs become associated with PTP1B$^{D/A}$. Therefore, consistent with a recent study showing that EGFR inactivation precedes degradation (*29*), our data show that most, if not all, incoming RTKs transit a "dephosphorylation compartment" before targeting to the lysosome or recycling to the plasma membrane. Functional imaging techniques such as those presented here should permit further elucidation of the spatiotemporal organization of PTP function and help us to understand how, where, and when these other negative regulatory processes function within the cell.

References and Notes

1. A. J. Flint, T. Tiganis, D. Barford, N. K. Tonks, *Proc. Natl. Acad. Sci. U.S.A.* **94**, 1680 (1997).
2. B. J. Goldstein, F. Ahmad, W. Ding, P. M. Li, W. R. Zhang, *Mol. Cell. Biochem.* **182**, 91 (1998).
3. M. Elchebly *et al.*, *Science* **283**, 1544 (1999).
4. L. D. Klaman *et al.*, *Mol. Cell. Biol.* **20**, 5479 (2000).
5. F. G. Haj, B. G. Neel, unpublished data.
6. J. V. Frangioni, P. H. Beahm, V. Shifrin, C. A. Jost, B. G. Neel, *Cell* **68**, 545 (1992).
7. T. A. Woodford-Thomas, J. D. Rhodes, J. E. Dixon, *J. Cell Biol.* **117**, 401 (1992).
8. Z. Y. Zhang, D. Maclean, D. J. McNamara, T. K. Sawyer, J. E. Dixon, *Biochemistry* **33**, 2285 (1994).
9. J. B. Bliska, J. C. Clemens, J. E. Dixon, S. Falkow, *J. Exp. Med.* **176**, 1625 (1992).
10. N. K. Tonks, B. G. Neel, *Curr. Opin. Cell Biol.* **13**, 182 (2001).
11. A. J. Garton, A. J. Flint, N. K. Tonks, *Mol. Cell. Biol.* **16**, 6408 (1996).
12. Primary mouse embryonic fibroblasts were generated from day 14 PTP1B-deficient mouse embryos and immortalized by infection with a retroviral vector expressing SV40 large T antigen. Immortalized PTP1B$^{-/-}$ cells were subsequently reconstituted with WT or D181A PTP1B cloned into the retroviral vector, pWZL Hygro. Pools of hygromycin-resistant cells, over 95% of which express PTP1B (as revealed by immunostaining), were used for the experiments. All cells were cultured in Dulbecco's modified Eagle's medium supplemented with 10% fetal calf serum, penicillin (100 U/ml), and streptomycin (10 mg/ml).
13. Supplementary material is available on *Science* Online at www.sciencemag.org/cgi/content/full/295/5560/1708/DC1.
14. T. W. J. Gadella Jr., T. M. Jovin, R. M. Clegg, *Biophys. Chem.* **48**, 221 (1993).
15. J. R. Lakowicz, K. Berndt, *Rev. Sci. Instrum.* **62**, 1727 (1991).
16. A. Squire, P. I. H. Bastiaens, *J. Microsc.* **193**, 36 (1999).
17. P. I. H. Bastiaens, A. Squire, *Trends Cell Biol.* **9**, 48 (1999).
18. P. J. Verveer, F. S. Wouters, A. R. Reynolds, P. I. H. Bastiaens, *Science* **290**, 1567 (2000).
19. FLIM sequences were obtained at a modulation frequency of 80 MHz with an Olympus IX70 microscope, using a 100×/1.4 numerical aperture (NA) oil objective. GFP was excited with a 476-nm Argon laser line, and fluorescence was detected with a dichroic beamsplitter (Q495 LP; Chroma Technology, Brattleboro, VT) and a narrow-band emission filter (HQ510/20; Chroma). Cy3 images were recorded with a 100-W Mercury arc lamp with a high Q Cy3 filter set (excite: HQ 545/30; dichroic: Q 580 LP; emitter: HQ 610/75).
20. F. S. Wouters, P. I. H. Bastiaens, *Curr. Biol.* **9**, 1127 (1999).
21. G. Huyer *et al.*, *J. Biol. Chem.* **272**, 843 (1997).
22. S. Sever, H. Damke, S. L. Schmid, *J. Cell Biol.* **150**, 1137 (2000).
23. A. V. Vieira, C. Lamaze, S. L. Schmid, *Science* **274**, 2086 (1996).
24. P. I. H. Bastiaens, I. V. Majoul, P. J. Verveer, H.-D. Söling, T. M. Jovin, *EMBO J.* **15**, 4246 (1996).
25. T. Finkel, *FEBS Lett.* **476**, 52 (2000).
26. J. Schlessinger, *Cell* **103**, 211 (2000).
27. G. Levkowitz *et al.*, *Mol. Cell* **4**, 1029 (1999).
28. C. A. Joazeiro *et al.*, *Science* **286**, 309 (1999).
29. P. Burke, K. Schooler, H. S. Wiley, *Mol. Biol. Cell* **12**, 1897 (2001).

30. We thank N. Tonks (Cold Spring Harbor Laboratory, NY) for PTP1B-expressing retroviral vectors, S. Schmid (Scripps Institute, CA) for the dominant-negative dynamin mutant, T. Rapoport and M. Rolls (Harvard Medical School) for anti-TRAPα antibodies and helpful discussions, V. Georget [European Molecular Biology Laboratory (EMBL), Heidelberg] for the PDGFR-GFP construct, and R. Saffrich (EMBL, Heidelberg) for help with microinjection of cells. We also thank L. Cantley and C. Carpenter for critical comments on the manuscript. This work was supported by NIH grant R01 CA49152 (to B.G.N.). F. Haj was aided by a mini-sabbatical award from the Harvard Digestive Diseases Center and P. Verveer was supported by a Marie Curie Fellowship of the European Community.

30 October 2001; accepted 9 January 2002

Discrete Microdomains with High Concentration of cAMP in Stimulated Rat Neonatal Cardiac Myocytes

Manuela Zaccolo* and Tullio Pozzan

The second messenger cyclic adenosine monophosphate (cAMP) is the most important modulator of sympathetic control over cardiac contractility. In cardiac myocytes and many other cell types, however, cAMP transduces the signal generated upon stimulation of various receptors and activates different cellular functions, raising the issue of how specificity can be achieved. In the general field of signal transduction, the view is emerging that specificity is guaranteed by tight localization of signaling events. Here, we show that in neonatal rat cardiac myocytes, β-adrenergic stimulation generates multiple microdomains with increased concentration of cAMP in correspondence with the region of the transverse tubule/junctional sarcoplasmic reticulum membrane. The restricted pools of cAMP show a range of action as small as approximately 1 micrometer, and free diffusion of the second messenger is limited by the activity of phosphodiesterases. Furthermore, we demonstrate that such gradients of cAMP specifically activate a subset of protein kinase A molecules anchored in proximity to the T tubule.

cAMP has been regarded as a freely diffusible second messenger (*1*) that mediates the action of a number of different receptors and modulates many cellular functions, as diverse as movement, growth, metabolism, and synaptic plasticity. In the heart, cAMP generated upon β-adrenergic receptor (β-AR) stimulation controls strength, duration, and frequen-

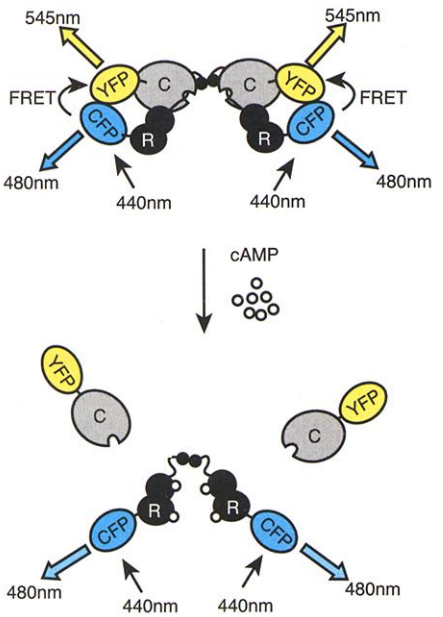

Fig. 1. Schematic illustration of the genetically encoded cAMP probe. The probe was generated by fusing R and C subunits of PKA to CFP and YFP, respectively, and takes advantage of the phenomenon of FRET. In conditions of low cAMP, the GFP-tagged PKA is found in its inactive holotetrameric conformation CFP-R_2C_2-YFP and FRET is maximal; upon excitation of the donor CFP at its proper excitation wavelength (440 nm), part of its excited-state energy is transferred to the acceptor YFP that then emits at its own wavelength (545 nm). When cAMP rises, the second messenger binds to R, inducing a conformational change that releases active C; CFP and YFP diffuse apart and FRET is abolished. FRET can be conveniently measured as the ratio of donor (480 nm) over acceptor emission (545 nm) intensities when cells are excited at the donor excitation wavelength (440 nm). Changes in fluorescence ratio (480 nm/545 nm) are directly correlated to changes in C and R subunit association and thus to cAMP level. The R and C subunits of PKA are shown in black and gray, respectively. Black straight arrows represent excitation; yellow and cyan arrows represent YFP and CFP emission, respectively. Peak excitation and emission intensities are also indicated.

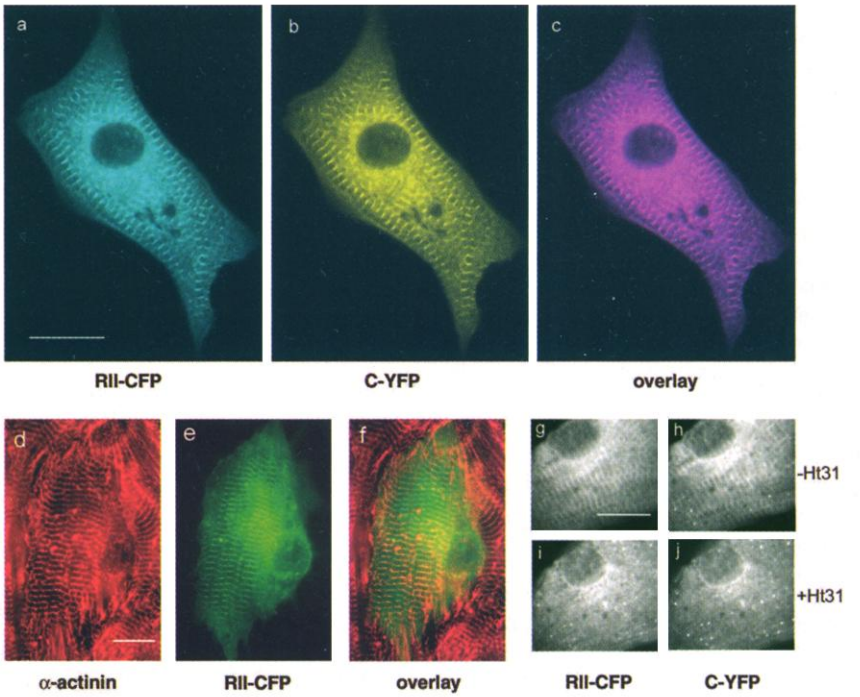

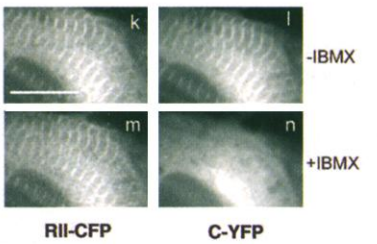

Fig. 2. Neonatal cardiac myocytes transfected with RII-CFP (**A**) and C-YFP (**B**). The colocalization of the two fluorescent PKA subunits is shown in (**C**). Cardiac myocytes cotransfected with RII-CFP (**E**) and C-YFP (not shown) and decorated with a monoclonal antibody specific for α-actinin (Sigma) (**D**). In (**F**), the images of (E) and (D) are superimposed; the yellow color indicates regions of overlapping signal. In (E), only the central cell is transfected. Cardiac myocytes cotransfected with RII-CFP [detail shown in (**G**)] and C-YFP (**H**) and treated with the myristoylated peptide Ht31 show the complete mobilization and diffusion in the cytosol of both PKA subunits [(**I**) and (**J**)]. Cardiac myocytes cotransfected with the cAMP sensor treated with 100 μM IBMX show the complete mobilization from striations and uniform distribution in the cytosol of C-YFP (**N**), whereas the addition of the PDE inhibitor has no effect on the segregation of RII-CFP (**M**). The same cell before IBMX addition is shown in (**K**) and (**L**). Bars = 10 μM.

cy of contraction. However, there are other receptors that transduce the signal via cAMP but generate functional effects that significantly differ from those elicited by β-AR (*2–4*). Thus, it remains to be clarified how stimulation of different receptors that act via the same second messenger can elicit the appropriate functional response.

An emerging view is that the spatial and temporal dynamics of the changes in concentration of the second messenger are part of the code that confers specificity (*5, 6*). The cAMP target enzyme, protein kinase A (PKA), is largely compartmentalized within the three-dimensional matrix of the cell via anchoring to A-kinase anchoring proteins (AKAPs) (*7*) and thus appears ideally suited to modulate cellular functions in response to local cAMP pools. In particular, in cardiac myocytes, the discrete distribution throughout the T tubular system of G_s heterotetrameric guanine nucleotide–binding proteins (*8*), adenylyl cyclases (ACs) (*8, 9*), AKAP-anchored PKA (*10*), and L-type Ca^{2+} channels (*9*), as well as the recent finding that phosphodiesterases (PDEs) can localize to specific subcellular domains via binding to AKAPs (*11*), provide a potential anatomical basis for the generation of cAMP compartments. Indeed, local generation of cAMP has been described (*12, 13*) and the range of action of the second messenger has been reported to be on the order of tens to hundreds of micrometers. The data presented here demonstrate that β-AR stimulation in cardiac myocytes generates multiple microdomains with a high concentration of cAMP with a range of action as small as ~1 μm. Such gradients selectively activate a pool of PKA molecules anchored to the T tubule membrane through AKAPs, thus providing a mechanism for β-AR selectivity.

We used a new version (*14*) of a previously described cAMP probe (*15*) (Fig. 1). With such a probe we can monitor PKA regulatory (R) and catalytic (C) subunit dissociation due to a rise in the intracellular cAMP concentration, $[cAMP]_i$, by measuring changes in fluorescence resonance energy transfer (FRET) between the cyan (CFP) and yellow (YFP) variants of green fluorescent protein (GFP). Primary cultures of ventricular cardiac myocytes from neonatal rats (*16*) transfected with both RII-CFP and C-YFP show, in addition to a diffuse distribution of the probe in the cytosol, a strong signal localized in thin parallel striations (*17*). Both R-CFP and C-YFP localized along these lines (Fig. 2, A through C). Cells transfected with CFP and YFP did not show such striated

Department of Biomedical Sciences and Venetian Institute for Molecular Medicine, University of Padua, Via Orus 2, 35129 Padua, Italy.

*To whom correspondence should be addressed. E-mail: manuela.zaccolo@unipd.it

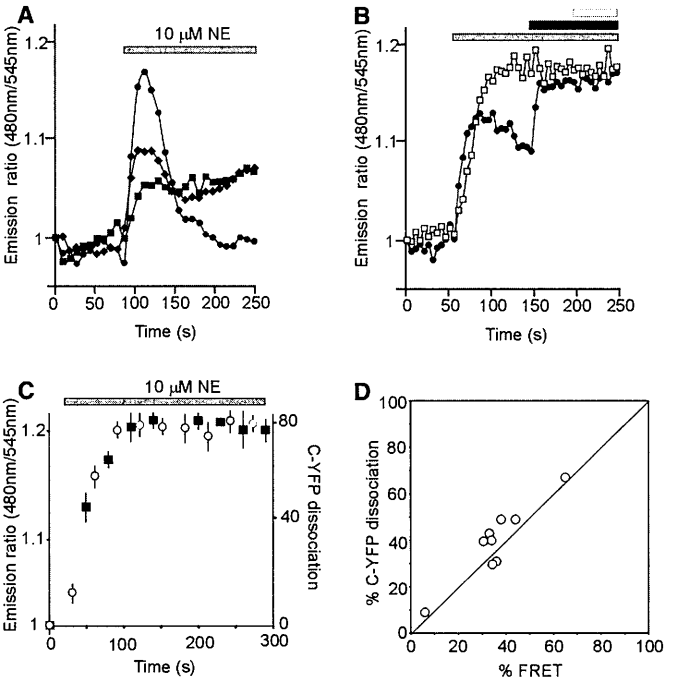

Fig. 3. (**A**) Kinetics of fluorescence ratio changes (480 nm/545 nm) recorded in neonatal cardiac myocytes cotransfected with RII-CFP and C-YFP and challenged with 10 μM NE (we tested increasing concentrations of NE on the same cell and found 10 μM to be a supramaximal dose). The graph shows three different responses recorded on independent cells. (**B**) Kinetics of fluorescence ratio changes recorded on cells that were either stimulated with 10 μM NE and subsequently with 100 μM IBMX and then forskolin (circles) or with 100 μM IBMX first and subsequently with 10 μM NE and then forskolin (squares). Gray and black bars represent first and second stimulus, respectively. White bar indicates addition of 25 μM forskolin. Figures in (A) and (B) are the mean of the intensity values calculated over the total area of a cell. The 480 nm/545 nm ratio in unstimulated cells varied in different experiments between 1 and 1.3 probably reflecting slight variations in the expression level of either subunit. To better compare different experiments, the basal ratio in (A) and (B) was therefore normalized to 1. (**C**) Kinetics of 480 nm/545 nm ratio changes (squares) and of C-YFP mobilization from striations (circles) recorded upon addition of 10 μM NE in one representative cell. Figures are the mean value calculated over six striations of this same cell. Bars indicate standard errors. Identical results were found in nine different cells. C-YFP mobilization was measured by exciting YFP at 500 nm and recording the emission fluorescence at 545 nm over the striation of interest. (**D**) Plot of FRET response versus C-YFP mobilization calculated as percent of the maximum recorded upon further addition of 100 μM IBMX. Circles represent independent cells.

patterns. The morphology and the distance (about 2 μm) between striations suggest that they might correspond to sarcomeric Z lines. Indeed, cardiac myocytes transfected with both RII-CFP and C-YFP and labeled with a monoclonal antibody to the Z line–specific protein α-actinin showed that the distribution of R-CFP [and C-YFP (*18*)] corresponded to that of α-actinin (Fig. 2, D through F). In adult cardiac myocytes, AKAPs are also present along T tubules (*10*), where they anchor PKA via binding to the RII subunit. In order to investigate if the GFP-tagged PKA was indeed anchored to AKAPs, we treated cells transfected with R-CFP and C-YFP with the membrane-permeable, PKA-anchoring inhibitor peptide Ht31 (*19*). After incubation of transfected cells with 150 μg/ml Ht31 for 30 min, the striated pattern disappeared and both PKA subunits were uniformly distributed in the cytosol (Fig. 2, G through J).

The distribution of the GFP-tagged PKA subunits showed a dynamic response to $[cAMP]_i$ increases. Double imaging of RII-CFP and C-YFP shows that addition of isobutyl-methyl-xanthine (IBMX) (100 μM), a broad spectrum PDE inhibitor, induced complete dissociation of C-YFP from RII-CFP at the striation whereas it had no effect on the localization of RII-CFP (Fig. 2, K through N). This effect was slowly reversible after removal of IBMX (*18*). The same complete and reversible dissociation of C-YFP was induced by 25 μM forskolin (*18*).

We analyzed fluctuations in $[cAMP]_i$ by measuring the kinetics of FRET changes in cells treated with agents that increase $[cAMP]_i$ (*20*). In 54 cells stimulated with 10 μM NE, about 10% showed no change in FRET whereas in the remaining 90%, we recorded a rise in FRET with a time for half maximal response ($t_{1/2}$) of 11.02 s ± 6.0 (±SD, n = 54). In 70% of the responding cells, the FRET change was transient (back to basal within 100 to 300 s), the time to reach

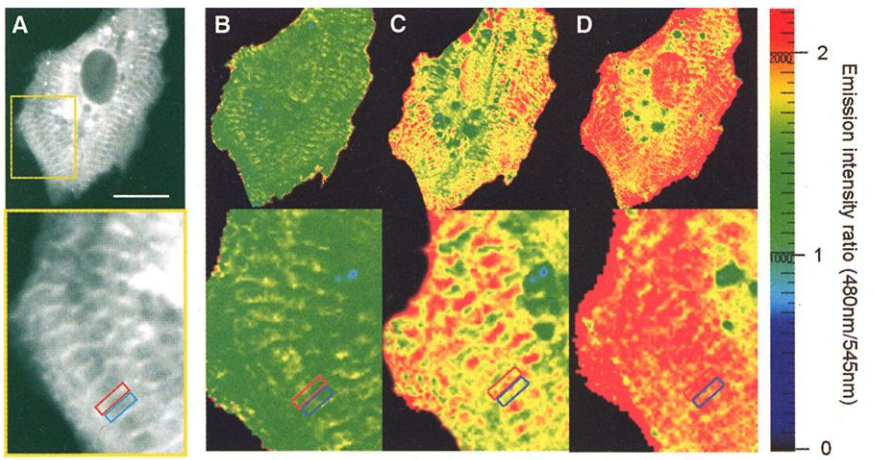

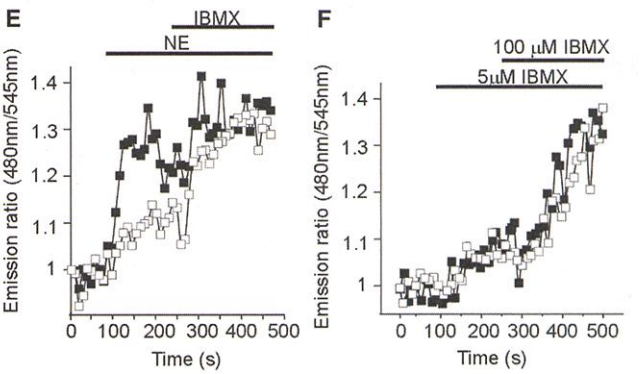

Fig. 4. Localized increases of cAMP. Cells were cotransfected with RII-CFP and C-YFP. (**A**) distribution pattern of C-YFP. The distribution of RII-CFP was identical. Bar = 10 μM. (**B** through **D**) the ratio image (480 nm/545 nm) of the same cell is presented in pseudocolors. The color scale is shown on the right. (**E**) filled squares indicate the kinetics of 480 nm/545 nm changes calculated on a striation [red box in (A)] and open squares indicate the kinetics of 480 nm/545 nm changes in a corresponding area between striations [blue box in (A)]. (**F**) Kinetics of 480 nm/545 nm changes calculated over a striation (filled squares) and between striations (open squares) in a representative cell stimulated with 5 μM IBMX and, subsequently, 100 μMIBMX.

the maximal response (t_{max}) being 45 s ± 5.7; the remaining 30% of responding cells showed a sustained increase of FRET for at least 5 min. Fig. 3A shows representative examples of different kinetics recorded on three independent cells stimulated with 10 μM NE. The complete reversibility of the response indicates that the GFP-tagged PKA subunits reassociate when $[cAMP]_i$ decreases. The value of the basal ratio after the transient response to NE is thus not affected by reassociation of GFP-tagged PKA subunits with the endogenous ones. The amplitude of the FRET response to NE was also variable (Fig. 3, A and D), ranging from 5 to 90% of the maximal response generated by the combined stimulation with NE and 100 μM IBMX (see for a typical example Fig. 3B); under the latter condition, further addition of 25 μM forskolin had no effect (Fig. 3B). This marked cell-to-cell variability could have not been revealed by previously available methodologies based on cell population analysis. The increase in the intensity ratio observed upon β-adrenergic stimulation was paralleled by dissociation of C-YFP from RII-CFP at striations. Figure 3C shows, in one representative cell of nine analyzed, that the kinetics of FRET changes elicited by 10 μM NE are indistinguishable from the kinetics of C-YFP dissociation and, independently of the absolute efficacy of the stimulus (from 5 to 70% of maximal), the dissociation of C-YFP from striations varied proportionally to FRET (Fig. 3D).

When the cells were stimulated first with 100 μM IBMX, the change in FRET was only slightly slower than in cells stimulated with NE ($t_{1/2}$ = 17.98 s, SD ±9.7, n = 31) and was maximal (that is, no further increase was observed after subsequent addition of 10 μM NE and forskolin) (Fig. 3B). These results indicate that AC has a sustained constitutive activity and that the basal concentration of cAMP is maintained low through the activity of PDE. In fact, PDE inhibition by itself generates a rise in cAMP higher than that induced by maximal stimulation of β-AR.

Upon addition of NE, the changes in ratio were compartmentalized within discrete subcellular regions, a much higher change being observed in regions corresponding to the striations and a much smaller effect in areas delimited by striations (Fig. 4, C and E); further addition of IBMX (100 μM) induced a rather uniform rise of the ratio (Fig. 4, D and E). In cells stimulated with 5 μM IBMX alone, the change in ratio observed appeared indistinguishable in the two areas (Fig. 4F). A similar uniform change in ratio was observed upon addition of 25 μM foskolin. In 63 cells analyzed, we found that when the cells were stimulated with 100 μM IBMX (n = 31) the FRET change between striations (measured at the peak of the response) was 98% ± 3 (SD) of that measured on striations. When the cells were stimulated with 5 μM IBMX (n = 7), the FRET change between striations was 101% ± 5 (SD) of that on striations. On the contrary, when the cells were stimulated with 10 μM NE (n = 25) the response in areas between striations was only 33% ± 6 (SD) of that on the striations. We conclude that, in neonatal cardiac myocytes, the activation of the β-AR generates locally a higher rise of cAMP in areas corresponding to T tubules/junctional SR membrane compared to the deeper cytosol. Diffusion of cAMP and equilibration of its concentration within the cytosol is prevented by the activity of PDEs; indeed, their inhibition dissipates the cAMP gradients and allows generalized activation of PKA.

To gain insight into the potential physiological role of local compartments of high cAMP, we generated a variant of the cAMP sensor not anchored to AKAPs. The modified sensor results from the deletion of the NH_2-terminal domain of RII, which includes the AKAP-binding domain (*21*). Ventricular myocytes transfected with the deleted GFP-tagged PKA showed no selective localization of the probe (Fig. 5, A and B). To directly verify that the deletion does not grossly alter the affinity for cAMP, we transfected Cos-7 cells with C-YFP and either ΔRII-CFP or the full-length RII-CFP subunit. The two probes were similarly distributed, and upon stimulation with NE the kinetics and the amplitude of response were comparable (Fig. 5C). Similarly, the response in terms of FRET changes to increasing amounts of forskolin was similar (Fig. 5C, inset). On the contrary, when cardiac myocytes were transfected with the deleted probe, the change in emission ratio in response to NE was reduced compared to controls transfected with the full-length probe (Fig. 5D). Further addition of IBMX resulted in a maximal FRET change, comparable to that obtained with the anchored cAMP sensor (Fig. 5D). For the 40 cells transfected with full-length GFP-tagged PKA that we analyzed for this set of experiments, the response to 10 μM NE was below 5% of the maximal response in 12% of the cells and ranged between 30 and 90% of maximum in 83% of the cells (Fig. 5E). On the contrary, 70% of the 42 myocytes transfected with C-YFP and ΔRII-CFP gave a response to NE below 5% of maximum, whereas the remaining 30% showed a response ranging from 5 to 30% of maxi-

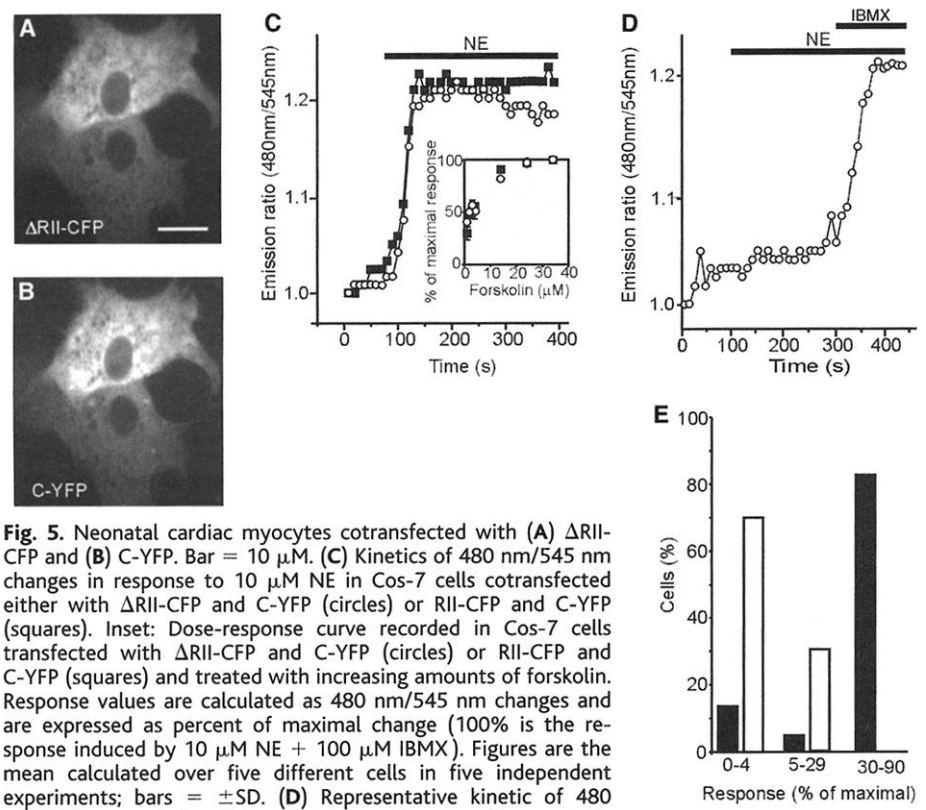

Fig. 5. Neonatal cardiac myocytes cotransfected with (**A**) ΔRII-CFP and (**B**) C-YFP. Bar = 10 μM. (**C**) Kinetics of 480 nm/545 nm changes in response to 10 μM NE in Cos-7 cells cotransfected either with ΔRII-CFP and C-YFP (circles) or RII-CFP and C-YFP (squares). Inset: Dose-response curve recorded in Cos-7 cells transfected with ΔRII-CFP and C-YFP (circles) or RII-CFP and C-YFP (squares) and treated with increasing amounts of forskolin. Response values are calculated as 480 nm/545 nm changes and are expressed as percent of maximal change (100% is the response induced by 10 μM NE + 100 μM IBMX). Figures are the mean calculated over five different cells in five independent experiments; bars = ±SD. (**D**) Representative kinetic of 480 nm/545 nm emission intensity changes in a cardiac myocyte cotransfected with ΔRII-CFP and C-YFP upon stimulation with 10 μM NE and subsequent addition of 100 μM IBMX. (**E**) Comparison between the fluorescence ratio change in response to 10 μM NE recorded in cells cotransfected with RII-CFP and C-YFP (black bars, n = 40) or ΔRII-CFP and C-YFP (white bars, n = 42). The response is expressed as percent of the maximal response, as recorded after further addition of 100 μM IBMX. n = number of independent cells analyzed.

mum. None of the cells expressing ΔRII-CFP responded with increased $[cAMP]_i$ above 30% of the maximum (Fig. 5E). These results indicate that only the GFP-tagged PKA anchored to AKAPs can efficiently sense the localized change in $[cAMP]_i$ induced by β-AR stimulation.

The hypothesis of compartments of high $[cAMP]_i$ in cardiac myocytes was formulated more than 20 years ago (*4, 22*), and restricted pools of cAMP appear to function in catecholamines-mediated control of cardiac Ca^{2+} channels (*13*). Our data provide direct evidence of microdomains of high cAMP and demonstrate that cAMP can act with a short range of about 1 μm.

References and Notes

1. T. Hunter, *Cell* **100**, 113 (2000).
2. J. S. Hayes, L. L. Brunton, S. E. Mayer, *J. Biol. Chem.* **255**, 5113 (1980).
3. J. S. Hayes, N. Bowling, K. L. King, G. B. Boder, *Biochem. Biophys. Acta* **714**, 136 (1982).
4. I. L. Buxton, L. L. Brunton, *J. Biol. Chem.* **258**, 10233 (1983).
5. S. F. Steinberg, L. L. Brunton, *Annu. Rev. Pharmacol. Toxicol.* **41**, 751 (2001).
6. D. M. F. Cooper, N. Mons, J. W. Karpen, *Nature* **374**, 421 (1995).
7. R. V. Schillace, J. D. Scott, *J. Clin. Invest.* **103**, 761 (1999).
8. M. A. Laflamme, P. L. Becker, *Am. J. Physiol.* **277**, H1841 (1999).
9. T. Gao *et al.*, *J. Biol. Chem.* **272**, 19401 (1977).
10. J. Yang, J. A. Drazba, D. G. Ferguson, M. A. Bond, *J. Cell Biol.* **142**, 511 (1998).
11. K. L. Dodge *et al.*, *EMBO J.* **20**, 1921 (2001).
12. B. J. Bacskai *et al.*, *Science* **260**, 222 (1993).
13. J. Jurevicius, R. Fischmeister, *Proc. Natl. Acad. Sci. U.S.A.* **93**, 295 (1996).
14. RII-CFP and C-YFP were generated by polymerase chain reaction (PCR) amplification of the cyan mutant and a pH-insensitive yellow mutant, respectively, of GFP (kindly provided by R. Tsien, University of California, San Diego, San Diego, CA), by using the forward primer 5′-TAACCAAGCTTA-ATGGTGAGCAAGGGC-3′ and the reverse primer 5′-CGCGGATCCTTACTTGTTCAGCTC-3′. The amplification products were cloned in frame at the 3′-end of the PKA subunits in the constructs RII-EBFP (*15*) and C-S65T (*15*) in place of EBFP and S65T, respectively. Both chimeras were then cloned into pCDNA3 (Invitrogen) as Hind III/Xba I fragments. ΔRII-CFP was generated by Pst I digestion and religation of pCDNA3–RII-CFP. The in-frame ablation of the Pst I fragment results in the deletion of a polypeptide that spans amino acids 15 to 40 in the RII subunit.
15. M. Zaccolo *et al.*, *Nature Cell Biol.* **2**, 25 (2000).
16. Cardiac ventricular myocytes from 1- to 3-day-old Crl:(WI)BR-Wistar rats (Charles River Laboratories, Wilmington, MA) were prepared as described (*23*). Briefly, ventricular tissue was enzymatically dissociated and the resultant cell suspension was plated onto 24-mm glass coverslips coated with laminin (Roche) and cultured in Dulbecco's modified Eagle's medium (DMEM) supplemented with 10% horse serum (HS) and 5% newborn calf serum (NCS). After 24 hours of culture, the medium was changed with DMEM supplemented with 5% HS and 0.5% NCS, and cells were transiently transfected with FuGene 6 (Roche) as described (*15*). All experiments were performed 36 to 48 hours after transfection in HEPES-buffered saline supplemented with 1 g $liter^{-1}$ glucose. All experiments were carried out at 37°C, and all chemicals were analytical grade.
17. Imaging of transfected cells was performed on a Zeiss Axiovert 100TX equipped with a CCD camera (T.I.L.L. Photonics GmbH, Martinsried, Germany) (Polychrome IV, T.I.L.L. Photonics GmbH), a software-controlled monochromator on the excitation side, and a filter wheel on the emission side. For RII-CFP imaging, transfected cells were excited at 440 nm, and fluorescence emission was collected using a 480DF30 emission filter (the dichroic mirror used was a 455DRLP). For C-YFP imaging, the excitation wavelength was 500 nm, the dichroic mirror was 525DRLP, and the emission filter was 545RDF35. All dichroics and emission filters are from Omega Optical.
18. M. Zaccolo, T. Pozzan, unpublished results.
19. D. V. Carr, Z. E. Hausken, I. D. Fraser, R. E. Stofko-Hahn, J. D. Scott, *J. Biol. Chem.* **267**, 13376 (1992).
20. FRET changes were measured as changes in the 480 nm/545 nm emission intensity using the software TillvisION v3.3 (T.I.L.L. Photonics GmbH) from the fluorescence images collected at 480 nm and 545 nm upon excitation of the cell at 440 nm (the dichroic mirror was a 455DRLP). For ratio calculation the background fluorescence was subtracted from each image. The integration time was 50 to 100 ms.
21. Y. Li, C. S. Rubin, *J. Biol. Chem.* **270**, 1935 (1995).
22. L. L. Brunton, J. S. Hayes, S. E. Mayer, *Adv. Cyclic Nucleotide Res.* **14**, 391 (1981).
23. D. E. Dostal, K. N. Rothbhlum, M. I. Chernin, G. R. Coope, K. M. Baker, *Am. J. Physiol.* **263**, C838 (1992).

24. We thank R. Tsien and S. Taylor for helpful discussion, S. Taylor for providing the PKA-anchoring inhibitory peptide Ht31, C. Destro for plasmid construction, V. Robert for help with myocyte primary cultures and discussion, and G. Ronconi, M. Santato, F. Cocco, M. Mongillo, and V. Toffolo for technical assistance. This work was supported by grants from Telethon-Italy, from the Italian Association for Cancer Research (AIRC), from the European Community, from the Italian Minister of University and Scientific Research (MURST), from the CNR (Target Project Biotechnology), and from the Armenise Harvard Foundation. M.Z. is an Assistant Telethon Scientist.

17 January 2002; accepted 25 January 2002

Structural Basis of Gating by the Outer Membrane Transporter FecA

Andrew D. Ferguson,[1] Ranjan Chakraborty,[2,3] Barbara S. Smith,[1] Lothar Esser,[1,4] Dick van der Helm,[2,5] Johann Deisenhofer[1]*

Siderophore-mediated acquisition systems facilitate iron uptake. We present the crystallographic structure of the integral outer membrane receptor FecA from *Escherichia coli* with and without ferric citrate at 2.5 and 2.0 angstrom resolution. FecA is composed of three distinct domains: the barrel, plug, and NH_2-terminal extension. Binding of ferric citrate triggers a conformational change of the extracellular loops that close the external pocket of FecA. Ligand-induced allosteric transitions are propagated through the outer membrane by the plug domain, signaling the occupancy of the receptor in the periplasm. These data establish the structural basis of gating for receptors dependent on the cytoplasmic membrane protein TonB. By compiling available data for this family of receptors, we propose a mechanism for the energy-dependent transport of siderophores.

Despite its relative abundance in Earth's crust, iron is biologically unavailable in an oxidizing atmosphere because of the insolubility of ferric oxyhydroxide. In response to iron deficiency, most microbes secrete organic chelators called siderophores, which are designed to sequester ferric iron. The ability to acquire this metal is an important determinant of bacterial virulence. Most bacteria express a sophisticated repertoire of parallel iron acquisition systems (*1*), which underscores their biological importance and the clinical potential to exploit these pathways for combating multi–drug-resistant bacterial strains (*2*).

Regulatory mechanisms, responsive to both the internal and external iron concentration, control the transcription of genes involved in iron uptake (*3*). The ferric citrate uptake (*fec*) genes are responsible for the transport of ferric citrate from the external medium into the cytoplasm (*4–7*). Proteins required for each phase of these energy-dependent transport processes have defined functions and are localized to specific cell envelope compartments. Embedded within the outer membrane is FecA, which performs two mutually independent functions: It binds and transports ferric citrate, and it is required to initiate transcription of the *fecABCDE* transport operon but not the regulatory *fecIR* genes (*4–7*). Both siderophore transport and the initiation of transcription require the

[1]Howard Hughes Medical Institute and Department of Biochemistry, University of Texas Southwestern Medical Center, 5323 Harry Hines Boulevard, Dallas, TX 75390, USA. [2]Department of Chemistry and Biochemistry, University of Oklahoma, 620 Parrington Oval, Norman, OK 73019, USA. [3]Department of Health Sciences, College of Public and Allied Health, East Tennessee State University, Post Office Box 70673, Johnson City, TN 37614, USA. [4]Laboratory of Cell Biology, National Cancer Institute, National Institutes of Health, 37 Convent Drive, Bethesda, MD 20892, USA. [5]Department of Biochemistry and Microbiology, University of Victoria, Post Office Box 3055, Victoria, British Columbia V8W 3P6, Canada.

*To whom correspondence should be addressed. E-mail: johann.deisenhofer@utsouthwestern.edu